Talanta 95 (2012) 18–24

Contents lists available at SciVerse ScienceDirect

Talanta

journal homepage: www.elsevier.com/locate/talanta

Fabrication of a methanol chemical sensor based on hydrothermally prepared α-Fe_2O_3 codoped SnO_2 nanocubes

Mohammed M. Rahman[a,b,*], Sher Bahadar Khan[a,b], A. Jamal[c], M. Faisal[c], Abdullah M. Asiri[a,b]

[a] Center of Excellence for Advanced Materials Research (CEAMR), King Abdulaziz University, P.O. Box 80203, Jeddah 21589, Saudi Arabia
[b] Chemistry Department, Faculty of Science, King Abdulaziz University, P.O. Box 80203, Jeddah 21589, Saudi Arabia
[c] Department of Chemistry & Center for Advanced Materials and Nano-Engineering (CAMNE), Faculty of Sciences and Arts, Najran University, P.O. Box 1988, Najran, 11001, Saudi Arabia

ARTICLE INFO

Article history:
Received 3 February 2012
Received in revised form 8 March 2012
Accepted 15 March 2012
Available online 21 March 2012

Keywords:
α-Fe_2O_3 codoped SnO_2 NCs
Optical properties
Structural properties
Methanol chemical sensor
Sensitivity
I–V method

ABSTRACT

We have prepared calcined α-Fe_2O_3 codoped SnO_2 nanocubes (NCs) by a hydrothermal method using reducing agents in alkaline medium. The codoped NCs were characterized by UV/vis, FT-IR, and Raman spectroscopy, powder X-ray diffraction (XRD), and field-emission scanning electron microscopy (FESEM). They were deposited on a silver electrode (AgE, surface area, 0.0216 cm^2) to give a sensor with a fast response towards methanol in liquid phase. The sensor also exhibits good sensitivity and long-term stability, and enhanced electrochemical response. The calibration plot is linear ($r^2 = 0.9809$) over the 0.25 mmol L^{-1} to 0.25 mol L^{-1} methanol concentration range. The sensitivity is ~5.79 μA cm^{-2} mM^{-1}, and the detection limit is 0.16 ± 0.02 mmol L^{-1} (signal-to-noise ratio, at a SNR of 3). We also discuss possible future prospective uses of this codoped semiconductor nanomaterial in terms of chemical sensing.

1. Introduction

Transition-metal doped semiconductor material is extensively used as liquid crystal displays, ferroelectric thin-film transistors, catalysts, gas-sensors, chemi-sensors, bio-sensors, and solar-cell applications [1–11]. SnO_2 is an n-type metal oxide which has large band-gap for codoped semiconductor oxides utilizing in spintronic applications. The use of carrier spin in codoped nanomaterials appears a new class of device such as polarized light emitters, integrated-memory, micro-processor functions, and magnetic devices, which displayed gain as well as ultra-low power transistors [12–15]. It is also extensively used in a variety of thin-film applications due to wide band-gap n-type semiconductor (Eg = 3.5–4.0 eV) and low-electrical resistance with high optical transparency in visible and near-IR electromagnetic spectrum [16,17]. The coexistence of tin interstitials and oxygen vacancies in SnO_2 is provided a unique combination of optical and electrical properties [18]. The SnO_2 is typically favored as the host in sight of their exciting optical and electrical properties in widespread applicability. SnO_2 nanostructure doping with metals (and metal oxides) without changing optical transparency is the key means of controlling electrical conductivity [19]. The metal ions (three d-shell transition) as dopants with open d-shell electronic configurations have employed different physical properties of their host semiconductors [20]. Iron oxide is one of the significant dopants of SnO_2 to obtain good quality films for sensor applications in broad-scale. Transition-metal doped semiconductor nanomaterial films reducing resistivity with fairly high-electronic transmittance were reported elsewhere [21,22]. By iron-doping, oxygen vacancies are generated in single dimensional SnO_2. The oxygen vacancy has a great influence on the physical and chemical as well as electrical properties, which is also strongly attracted toward Fe-ions. As a consequence, the transition metal–oxygen vacancies of semiconductor groups are used as common dopant in SnO_2.

Iron-oxide codoped SnO_2 thin films were prepared by various techniques such as chemical vapor deposition, rf-sputtering, sol–gel spin coating, sol–gel dip coating, and sprays pyrolysis [23–27]. Among the various deposition techniques, the hydrothermal technique is the most convenient method due to the simplicity and inexpensive experimental arrangement, ease of doping materials, high-growth rate, and mass-production capability for industrial applications [28]. Several scientific reports have been published on nanomaterial films to detect the various toxic chemicals at room conditions. Cheng et al. have reported the gas-sensing properties of metal-oxide nano-particle thin-films to ethanol and propanol chemicals [29]. Arshak and Gaiden have measured the zinc and

* Corresponding author at: Center of Excellence for Advanced Materials Research (CEAMR) & Chemistry Department, Faculty of Science, King Abdulaziz University, P.O. Box 80203, Jeddah 21589, Saudi Arabia. Tel.: +966 596421830.
E-mail address: mmrahman@kau.edu.sa (M.M. Rahman).

0039-9140/$ – see front matter © 2012 Elsevier B.V. All rights reserved.
doi:10.1016/j.talanta.2012.03.027

silver oxide thick-film sensors to detect ethanol and propanol subsequently [30]. Methanol-sensing properties of CeO_2–Fe_2O_3 thin-films have been also executed by Neri et al. recently [31]. They have investigated that the addition of CeO_2 to Fe_2O_3 is enhanced the methanol response at low temperature. Indium tin oxide thin-film sensors for detection of methanol have been reported by Patel et al. at room temperature [32].

Here the calcined α-Fe_2O_3 codoped SnO_2 NCs have significant properties such as large surface area (surface-to-volume ratio), non-toxicity, chemical stability, and high electrical conductivity; which offered high electron communication features that enhanced the direct electron communication towards the target analytes. As methanol is highly carcinogenic and serious to health as well as environment, it is urgently required to fabricate a simple and reliable chemical sensor with doped semiconductor nanomaterials. Consequently, the methanol sensing properties of α-Fe_2O_3 codoped SnO_2 NCs films have been explained in term of fabrication and detection mechanism in this report. The simple fabrication technique is used for the preparation of doped thin-film NCs on AgE with conducting binders, which is measured by simple and reliable *I–V* method. To best of our knowledge, this is the first report for highly sensitive detection of methanol with calcined α-Fe_2O_3 codoped SnO_2 NCs using simple *I–V* technique in short response time.

2. Experimental details

2.1. Materials and methods

Analytical grade of methanol, ferric chloride, tin chloride, ethyl acetate, disodium phosphate (Na_2HPO_4), ammonia solution (25%), butyl carbitol acetate, and monosodium phosphate (NaH_2PO_4) was used and purchased from Sigma–Aldrich Company. Stock solution of 12.5 mol L^{-1} methanol was taken from the purchased chemical. The λ_{max} (423.0 nm) of calcined Fe_2O_3–SnO_2 NCs was evaluated with UV/visible spectroscopy (Lamda-950, Perkin Elmer, Germany). FT-IR spectra were performed with a spectrophotometer (Spectrum-100 FT-IR) in the mid-IR range, which was purchased from Perkin Elmer, Germany. Raman station 400 (Perkin Elmer, Germany) was used to measure the Raman shift of codoped NCs material using radiation source (Ar^+ laser line, λ: 513.4 nm). The powder X-ray diffraction (XRD) prototypes were assessed with X-ray diffractometer (X'Pert Explorer, PANalytical diffractometer) equipped with CuKα$_1$ radiation (λ = 1.5406 nm) using a generator voltage of 40.0 kV and a generator current of 35.0 mA applied for the purposed. Morphology of codoped nanomaterial was investigated on FESEM instrument (FESEM; JSM-7600F, Japan). *I–V* technique was executed by using Electrometer (Kethley, 6517A, Electrometer, USA) at room conditions.

2.2. Synthesis and growth mechanism of α-Fe_2O_3 codoped SnO_2 NCs

The solution of starting reactants ($FeCl_3$ and $SnCl_4{\cdot}2H_2O$) is prepared in aqueous medium at room conditions. After addition of NH_4OH (for adjusting the pH) into the mixture of metal chloride solutions, it was stirred gradually and powerfully for few minutes at room temperature. α-Fe_2O_3 codoped SnO_2 NCs have been prepared by adding uni-molar concentration of $FeCl_3$ and $SnCl_4$ as starting (reducing agent) materials into hydrothermal cell (Teflon line autoclave) for 16 h. Initially, reactants were gradually dissolved into the de-ionized water to form 0.1 mol L^{-1} concentration individually at room temperature. Then these uni-molar solutions were mixed properly and then the solution pH was adjusted (at 10.4) using aqueous NH_4OH; and finally placed into the oven at 150.0 °C for 16 h. The starting materials of $SnCl_4$, $FeCl_3$, and NH_4OH were used without further purification for co-precipitation technique to doped ($Fe_2O_3{\cdot}SnO_2$) composition. Again NH_4OH was added dropwise into the strongly stirred $SnCl_4$ and $FeCl_3$ solutions mixture to produce a significant doped precipitate.

The growth mechanism of α-Fe_2O_3 codoped SnO_2 nanostructure materials can be elucidated on the basis of chemical reactions and nucleation as well as growth of doped nanocrystals, which is presented in below.

$$NH_4OH_{(aq)} \rightarrow NH_4{}^+{}_{(aq)} + OH^-{}_{(aq)} \quad \text{(i)}$$

$$SnCl_4{\cdot}2H_2O + 4NH_4OH_{(aq)} + H_2O_{(aq)} \rightarrow Sn(OH)_{4(aq)} + 4NH_4Cl + 3H_2O_{(aq)} \quad \text{(ii)}$$

$$FeCl_{3(s)} + 3NH_4OH_{(aq)} \rightarrow Fe(OH)_{3(aq)} + 3NH_4{}^+{}_{(aq)} + 3Cl^-{}_{(aq)} \quad \text{(iii)}$$

$$FeCl_{3(s)} + 2NH_4OH_{(aq)} \rightarrow Fe(OOH)_{(aq)} + 2NH_4{}^+{}_{(aq)} + H^+{}_{(aq)} + 3Cl^-{}_{(aq)} \quad \text{(iv)}$$

$$2Fe(OH)_{3(aq)} + 4NH_4OH_{(aq)} + Sn(OH)_{4(aq)} \rightarrow Fe_2O_3{\cdot}SnO_{2(s)} + 4NH_4{}^+ + 9H_2O \quad \text{(v)}$$

$$Sn(OH)_{4(aq)} + 2Fe(OOH)_{(aq)} \rightarrow Fe_2O_3{\cdot}SnO_{2(s)} + 4H_2O \quad \text{(vi)}$$

The reaction is forwarded slowly according to the proposed Eqs. (i)–(iv). During preparation, the pH value of the reaction medium plays an important responsibility in the nanomaterial doped oxide formation. At a particular pH, when $SnCl_4$ is hydro-lyzed with basic solution (ammonium hydroxide), tin hydroxide is formed instantly according to Eq. (ii). During the synthesis of nanomaterials, NH_4OH is used to control the pH value (alkaline phase) as well as supplied the hydroxyl ions (OH^-) slowly in reaction system. When the concentration of Sn^{2+} and OH^- ions is reached to critical value, SnO_2 nuclei formation becomes started. As the high concentration of Fe^{3+} ions [reactions (iii) and (iv)], the nucleation of SnO_2 crystals become slower due to the lower activation energy barrier of heterogeneous nucleation. In presence of Fe^{3+} concentration in reaction system, a number of larger α-$Fe_2O_3{\cdot}SnO_2$ crystals with aggregated cube-like morphology were formed according to the reactions [Eqs. (v)–(vi)]. The shape of calcined $Fe_2O_3{\cdot}SnO_2$ NCs is reliable with the growth pattern of Fe_2O_3 codoped SnO_2 crystals [33]. Then the resultant solution was washed thoroughly with acetone, ethanol, and water consecutively and kept for drying at room conditions. Finally, the as-grown doped α-$Fe_2O_3{\cdot}SnO_2$ NCs materials were calcined at 400.0 °C for 5 h in the furnace (Barnstead Thermolyne, 6000 Furnace, USA). The calcined products were characterized in detail in terms of their morphological, structural, optical properties, and applied for methanol chemical sensing for the first time.

2.3. Preparation of phosphate buffer and analyte solution

0.1 mol L^{-1} phosphate buffer solution (PBS) at pH 7.0 is prepared by mixing of equi-molar concentration of 0.2 mol L^{-1} Na_2HPO_4 and 0.2 mol L^{-1} NaH_2PO_4 solution in 100.0 mL de-ionize water at room conditions. As received methanol (99.9%) is diluted to make various concentrations (0.25 mmol L^{-1} to 12.5 mol L^{-1}) in DI water and used as a target analyte. 10.0 mL of 0.1 mol L^{-1} PBS is kept constant during measurements.

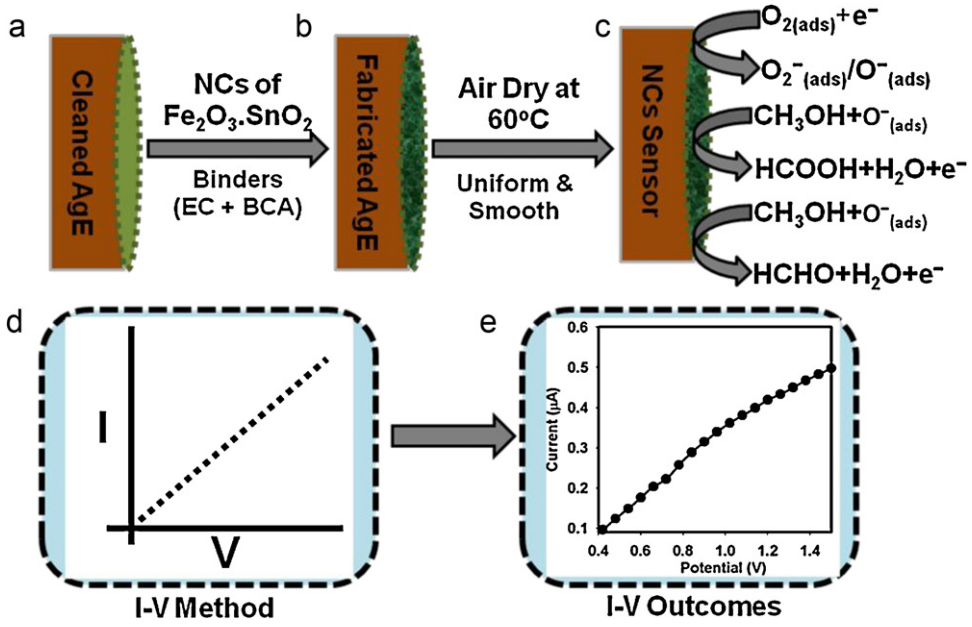

Scheme 1. Schematic view of (a–c) fabrication and proposed mechanism of methanol detection with codoped NCs modified AgE (NCs/AgE), (d) theoretical, (e) practical *I–V* methods in presence of α-Fe_2O_3 codoped SnO_2 semiconductor NCs.

2.4. Fabrication of AgE with α-Fe_2O_3 codoped SnO_2 NCs

Silver electrode (AgE) is fabricated with α-Fe_2O_3 codoped SnO_2 NCs using butyl carbitol acetate (BCA) and ethyl acetate (EA) as a conducting binder. Then it is kept in the oven at 60.0 °C for 3 h until the film is completely dried, stable, and smooth. A cell is assembled with NCs/AgE and Pd-wire as a working and counter electrodes respectively. The ratio of current vs. concentration (slope of calibration curve) is used to calculate the methanol sensitivity. Detection limit is evaluated from the ratio of 3N/S (ratio of Noise × 3 vs. Sensitivity) from the linear dynamic range of calibration curve. Electrometer is used as a constant voltage sources for *I–V* measurement in simple two electrode system. The calcined α-Fe_2O_3 codoped SnO_2 NCs are fabricated and employed for the detection of methanol in liquid phase. *I–V* response is measured with NCs/AgE film according to Scheme 1. Palladium (PdE) and silver electrode (AgE) are used as a counter and working electrode (voltage sources, in two electrode system) respectively, which is presented in Scheme 1a. The theoretical and experimental *I–V* detection methods with NCs using conducting binder are presented in Scheme 1b and c respectively. The proposed detection mechanism of fabricated methanol sensors using *I–V* responses is presented in Scheme 1d.

3. Results and discussions

3.1. Optical characterization

The optical property of the calcined α-Fe_2O_3 codoped SnO_2 NCs structure is one of the important characteristics for the evaluation of its photo-catalytic activity. The optical absorption spectra of NCs are measured by using UV–visible spectrophotometer in the visible range (200.0–800.0 nm). In UV/visible absorption technique, the outer electrons of atoms or molecules are absorbed by incident a radiation source, which undergoes electron transition from lower to higher energy levels. In this phenomenon, the spectrum obtained owing to optical absorption can be analyzed to acquire the energy band gap of the semiconductor nanomaterials [34]. The optical absorption measurement was carried out at ambient conditions. From the absorption spectrum, an absorbance maximum is measured using calcined doped NCs at 423.0 nm, which is presented in Fig. 1a. Band gap energy (E_{bg}) is calculated on the basis of the maximum absorption band of NCs and found to be 2.9314 eV, according to following Eq. (vii).

$$E_{bg} = \frac{1240}{\lambda}(\text{eV}) \qquad \text{(vii)}$$

where E_{bg} is the band-gap energy and λ_{max} is the wavelength (423.0 nm) of the NCs. No extra peak associated with impurities and structural defects were observed in the spectrums, which proved that the synthesized NCs control crystallinity of α-Fe_2O_3 codoped SnO_2 nanomaterials [35–37].

The calcined α-Fe_2O_3 codoped SnO_2 NCs are also studied in term of the atomic and molecular vibrations. To predict the motivated identification, FT-IR spectra basically in the region of 400–4000 cm^{-1} are investigated at room conditions. Fig. 1b displays the FT-IR spectrum of the calcined NC nanostructures. It represents band at 612, 1632, and 3424 cm^{-1}. These observed wide vibration band (at 612 cm^{-1}) could be assigned as metal–oxygen (Sn–O and Fe–O modes) stretching vibrations [38–41], which is demonstrated the configuration of codoped nanostructure materials. The supplementary vibrational bands may be assigned to O—H bending (1632 cm^{-1}) and O—H stretching (3424 cm^{-1}) vibrations. The absorption bands (1632 cm^{-1} and 3424 cm^{-1}) are exhibited from water, which generally semiconductor nanostructure materials absorb from the environment due to their mesoporous nature [42,43]. Finally, at low-frequency region, the vibrational band is suggested the formation of α-Fe_2O_3 codoped SnO_2 NCs.

Raman spectroscopy is used to disclose vibrational, rotational, and other low-frequency phases in Raman active compounds. It is constructed on inelastic scattering of mono-chromatic light in visible, near-infrared, or near-ultraviolet range (i.e., Raman scattering). Raman spectroscopy is generally known and exploited in material chemistry, since the information is explicit to the chemical bonds and symmetry of metal–oxygen stretching or vibrational modes. In Fig. 1c, the wave numbers were measured using Raman spectra at 222 cm^{-1}, 288 cm^{-1}, 408 cm^{-1}, 604 cm^{-1}, and 1302 cm^{-1}, which represents the metal–oxygen stretching vibrations (Fe–O

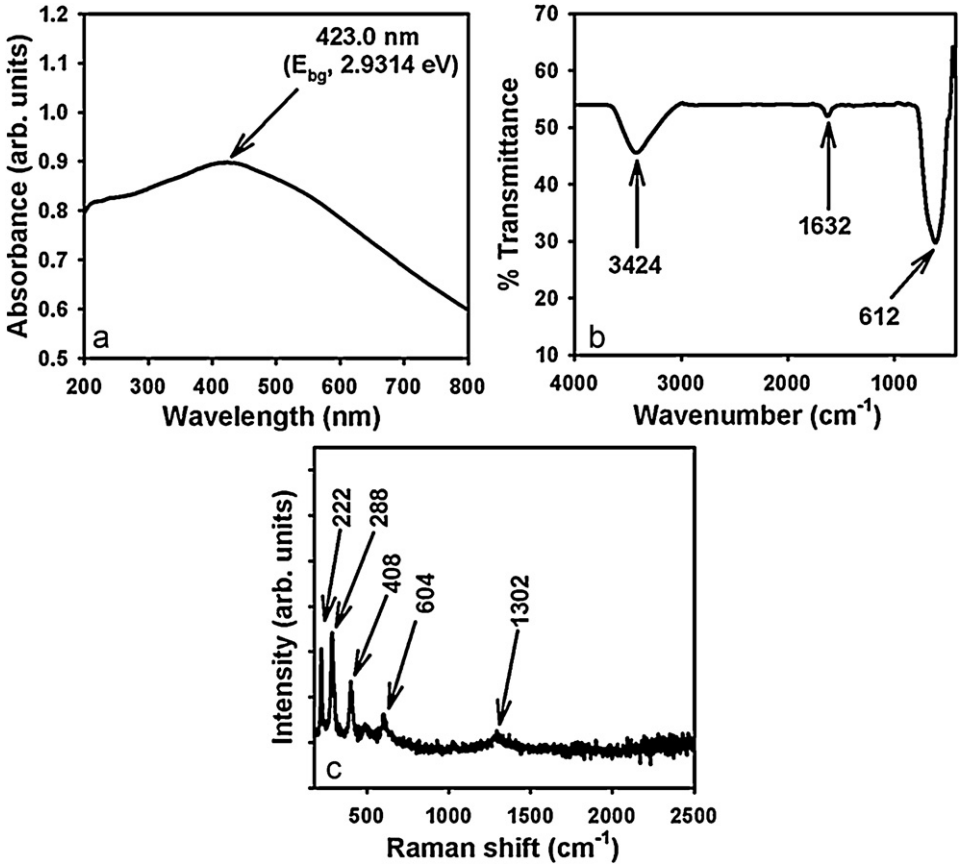

Fig. 1. Typical (a) UV–vis spectrum, (b) FT-IR spectrum, and (c) Raman spectrum of calcined α-Fe_2O_3 codoped SnO_2 NCs.

and Sn–O). These bands can be assigned to a cubic-phase of α-Fe_2O_3 codoped SnO_2 NCs [44].

3.2. Structural and morphological characterizations

The reflection peak is found to match with iron oxide phase (Hematite, α-Fe_2O_3) having Rhombohedral geometry [*Joint Committee on Powder Diffraction Standards*, JCPDS # 080-2377]. In Fig. 2a, the phases (with indices) are represented to the major characteristic peaks (black-color) for calcined crystalline iron oxide at 2θ values of 24.15(0 1 2), 33.16(1 0 4), 35.63(1 1 0), 49.46(0 2 4), 54.1(1 1 6), and 72.28(1 1 9) degrees. The lattice parameters are $a = 5.03521$; $c = 13.7505$, $Z = 6$, point group: R-3c(167), and radiation: Cu Kα_1 ($\lambda = 1.5406$). These indicate that there is considerable amount of crystalline iron oxide present in codoped nanomaterials. Beside α-Fe_2O_3, the reflection peaks were also found to match with SnO_2 phase (cassiterite) having tetragonal geometry [JCPDF # 072-1147]. The phases are showed the major characteristic peaks (blue-color) with indices for calcined crystalline SnO_2 at 2θ values of 26.59(1 1 0), 54.77(2 2 0), 62.6(2 2 1), and 64.77(1 1 2) degrees in Fig. 2a. The tetragonal (unit cell) lattice parameters are $a = 4.737$; $c = 3.185$; $Z = 2$, point group: P42/mnm(136), and radiation: Cu Kα_1 ($\lambda = 1.5406$). These indicate that there is considerable amount of crystalline SnO_2 present in codoped nanostructural materials. Finally, this X-ray pattern is corresponded to NCs sample, which may be attributed to the doping of NC lattice site of codoped aggregated NCs semiconductor materials [45–49]. Further, no other impurity peak was observed in the XRD pattern showing the α-Fe_2O_3 codoped SnO_2 NCs phase formation.

High resolution FESEM images of calcined α-Fe_2O_3 codoped SnO_2 NCs are exhibited in Fig. 2b–d. The FESEM images of aggregated nano-structural materials are displayed in cubic-shape. The average diameter of NCs is calculated in the range of 106.61∼338.15 nm, which is close to 205.64 ± 10.0 nm. It is clearly exhibited from FESEM that the synthesized codoped products are nanostructure of NCs. It is revealed in regular cubic-shape with high-density block-shape nanostructure. It is also proposed that the hydrothermally prepared nanostructures are composed in cubic-shape of aggregated α-Fe_2O_3 codoped SnO_2 NCs [50]. The crystalline size was also calculated and confirmed using Scherrer formula [51],

$$D = \frac{0.9\lambda}{\beta \cos\theta}$$

where λ is the wavelength of X-ray radiation, β is the full width at half maximum (FWHM) of the peaks at the diffracting angle θ. The average diameter of NCs (α-Fe_2O_3 codoped SnO_2 NCs) is close to ∼201.0 nm.

3.3. Methanol detection using I–V technique

The calcined α-Fe_2O_3 codoped SnO_2 NCs were employed for the detection of methanol in liquid phase. *I–V* responses were measured with NCs coated thin-film (in two electrodes system), which was presented in experimental sections. Scheme 1 already outlined the methanol sensing protocol using the NCs/AgE modified electrode. The concentration of methanol was varied from 0.25 mmol L^{-1} to 12.5 mol L^{-1} by adding de-ionized water at different proportions. Here, Fig. 3a is represented the *I–V* responses for uncoated-AgE (gray-dotted) and NCs-coated-AgE (black-dotted) electrodes. In PBS system, the NCs/AgE electrode shows that the reaction is reduced slightly owing to the presence of semiconductor NCs on bare-AgE surface. A considerable enhancement of

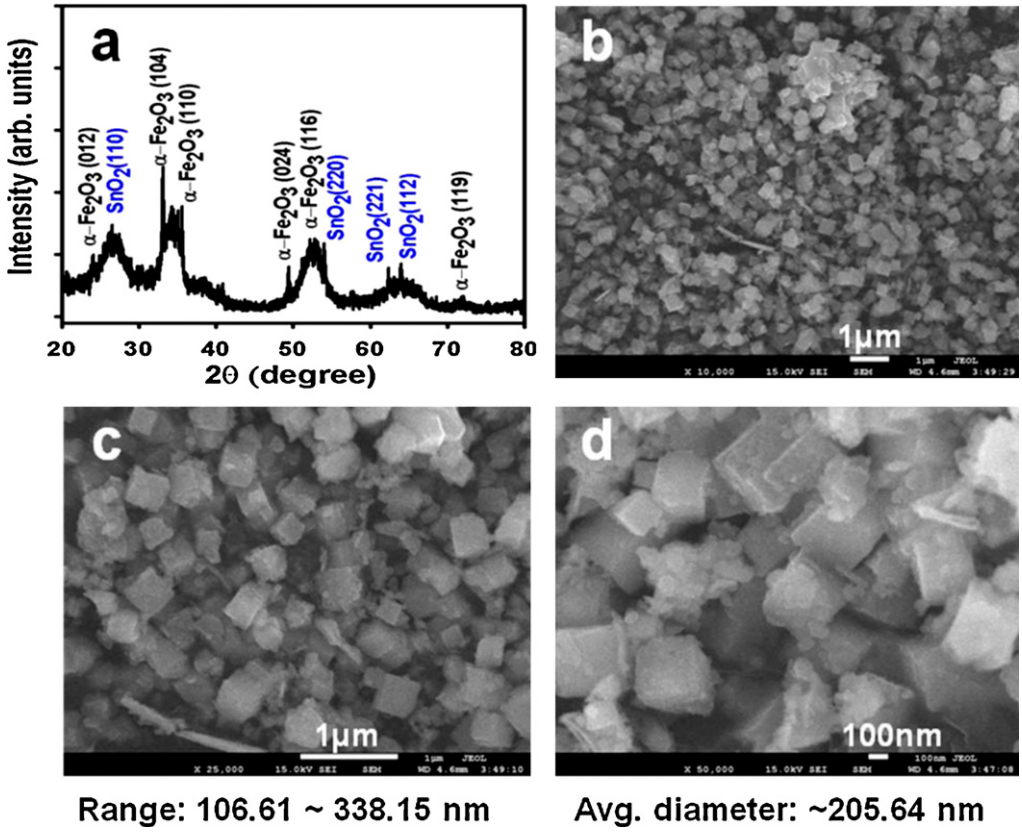

Fig. 2. (a) X-ray powder diffraction and (b–d) low to high-magnified FESEM images of calcined α-Fe_2O_3 codoped SnO_2 NCs. (For interpretation of the references to color in this figure legend, the reader is referred to the web version of the article.)

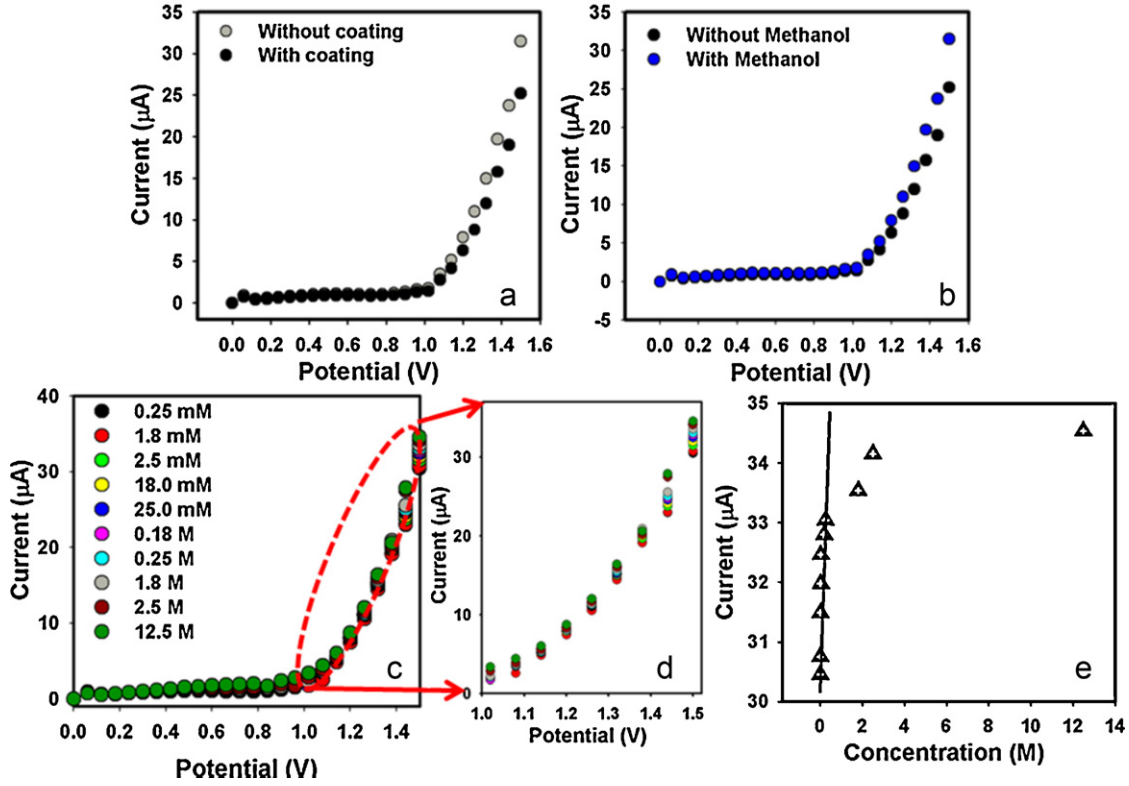

Fig. 3. *I–V* responses of: (a) AgE (without α-Fe_2O_3 codoped SnO_2 coating) and NCs/AgE (with α-Fe_2O_3 codoped SnO_2 coating); (b) NCs/AgE (in absence of methanol) and methanol/NCs/AgE (in presence of methanol); (c) concentration variations (0.25 mmol L^{-1} to 12.5 mol L^{-1}) of methanol, (d) magnified view of current responses between +1.0 and +1.5 V; (e) calibration plot of NCs fabricated silver electrode. (For interpretation of the references to color in this figure legend, the reader is referred to the web version of the article.)

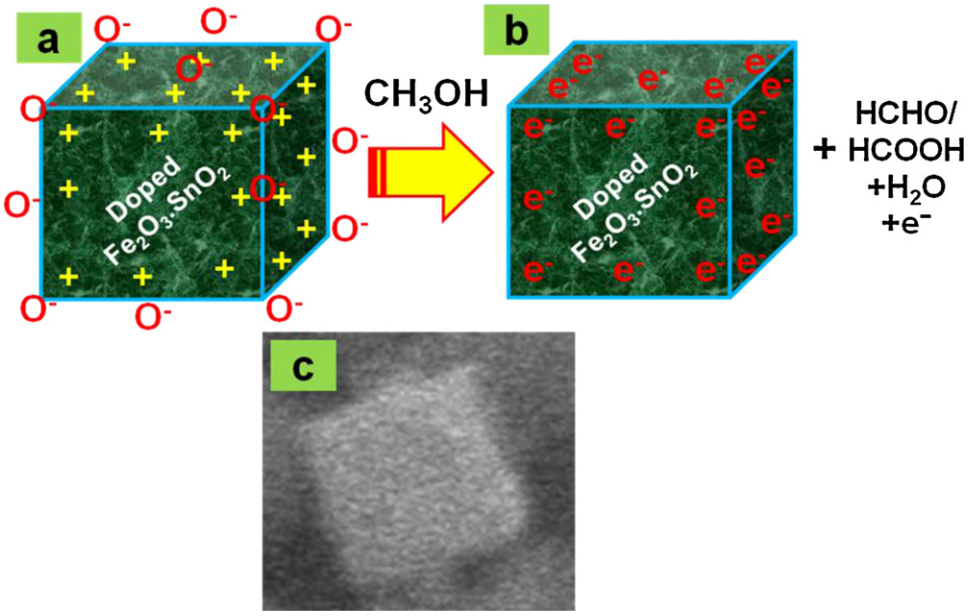

Fig. 4. Mechanism of methanol sensors based on calcined α-Fe_2O_3 codoped SnO_2 NC at room conditions. (a) Before reaction with methanol, (b) after reaction with methanol, and (c) real and magnified NC image.
Taken from Fig. 2c.

current value with applied potential is demonstrated with fabricated NCs/AgE in presence of target analyte, which is presented in Fig. 3b. The black-dotted and blue-dotted curves were indicated the response of the fabricated film before and after injecting 50.0 μL methanol in 10.0 mL PBS solution respectively. Significant increases of current are measured after injection of target component in regular interval. *I–V* responses to varying methanol concentration on thin NCs were investigated (time delaying, 1.0 s) and presented in Fig. 3c. The comparative plots (magnified-view) of resultant current of various concentrations between +1.0 and +1.5 V are separately presented in Fig. 3d.

Analytical parameters (such as sensitivity, detection limit, linearity, and linear dynamic range) were calculated from the calibration curve (current vs. concentration), which was presented in Fig. 3e. A wide range of methanol concentration was selected to study the possible detection limit (from calibration curve), which was examined in 0.25 mmol L^{-1} to 12.5 mol L^{-1}. The sensitivity was calculated from the calibration curve, which was close to 5.79 μA cm^{-2} mmol L^{-1}. The linear dynamic range of the NCs/AgE sensor was employed from 0.25 mmol L^{-1} to 0.25 mol L^{-1} (linearly, $r^2 = 0.9809$), where the detection limit was calculated about 0.16 ± 0.02 mmol L^{-1} (ratio, 3N/S). The NCs/AgE was exhibited semiconductor behaviors, where the electrical resistance decreases under the presence of reducing agent in solution phase. The film resistance was decreased gradually (increasing the resultant current) upon increasing the methanol concentration in bulk system.

I–V characteristic of the NCs is activated as a function of methanol concentration at room conditions, where improved current response is observed. As obtained, the current response of the NCs-film is increased with the increasing concentration of methanol, however similar phenomena has also been reported earlier [29,52]. For a low concentration of methanol in liquid medium, there is a smaller surface coverage of methanol molecules on α-Fe_2O_3 codoped SnO_2 NCs film and hence the surface reaction proceeds steadily. By increasing the methanol concentration, the surface reaction is increased significantly (gradually increased the response as well) owing to large surface area contacted with methanol molecules. Further increase of methanol concentration on NCs/AgE surface (low-dimensional crystalline size and low-lattice disorder), it is exhibited a more rapid increased the current responses, due to larger surface covered by methanol chemical. Usually, the surface coverage of methanol molecules on NCs/AgE surface is reached to saturation, based on the regular enhancement of current responses. The methanol-sensing mechanism of the NCs film is explained as follows.

Initially, oxygen (dissolved) is chemisorbed on the NCs/AgE surfaces, while NC coated-film electrode is immersed into PBS system. During the chemi-sorption, the dissolved oxygen is converted to ionic species (such as O_2^- and O^-) which is gained electrons from the conduction band of codoped NCs [53,54]. The reaction mechanism is presented in below [Eqs. (viii)–(x)] as well as in Fig. 4a.

$$O_{2(diss)} \rightarrow O_{2(ads)} \quad \text{(viii)}$$

$$O_{2(ads)} + e^- \rightarrow {O_2}^-{}_{(ads)} \quad \text{(ix)}$$

$${O_2}^-{}_{(ads)} + e^- \rightarrow 2{O}^-{}_{(ads)} \quad \text{(x)}$$

The reaction between methanol and ionic oxygen species is executed by two different ways [32], which are schematically presented in Fig. 4b and c.

$$CH_3OH_{(liq)} + {O}^-{}_{(ads)} \rightarrow HCHO + H_2O + e^- \quad \text{(xi)}$$

$$HCHO + 2O_{(bulk)} \rightarrow HCOOH + O_{(vac)} \quad \text{(xii)}$$

$$CH_3OH_{(liq)} + {O_2}^-{}_{(ads)} \rightarrow HCOOH + H_2O + e^- \quad \text{(xiii)}$$

Here, the reactions [Eqs. (xi)–(xiii)] are directly depended in presence of methanol into reaction system. On NCs/AgE surfaces, methanol is oxidized to convert as formaldehyde and formic acid, which is released electrons into the conduction band. Therefore it is decreased the resistance (increasing the conduction current) of the NCs film.

Actually the response time was around 10.0 s for the fabricated NCs/AgE to reach the saturated steady-state level. The higher sensitivity of the fabricated NCs/AgE could be attributed to the excellent absorption (porous surfaces in NCs/binders/AgE) and adsorption ability, high catalytic-decomposition activity, and good biocompatibility of the NCs. The estimated sensitivity of the fabricated sensor is relatively higher and detection limit is comparatively lower than previously reported methanol sensors based on other

nano-composite or nano-materials modified electrodes [55–59]. Due to high specific surface area, NCs provide a favorable micro-environment for the methanol detection with good quantity. The high sensitivity of NCs/AgE provides high electron communication features which enhanced the direct electron transfer between the active sites of codoped NCs and AgE. The NCs/AgE system is demonstrated a simple and reliable approach for the detection of toxic chemicals. It is also revealed that the significant access to a large group of chemicals for wide-range of ecological and biomedical applications in environmental and health-care fields respectively.

The methanol chemical sensor based on NCs is displayed good reproducibility and stability for over two weeks and no major changes in sensor responses are found. After two weeks, the chemical sensor response with doped NCs was slowly decreased, which may be due to the weak-interaction between fabricated NCs active surfaces and methanol chemical. The significant result was achieved by hydrothermally prepared α-Fe_2O_3 codoped SnO_2 NCs, which can be employed as proficient electron mediators for the development of efficient chemical sensors.

4. Conclusions

Finally, we have successfully fabricated methanol chemical sensor based on low-dimensional calcined α-Fe_2O_3 codoped SnO_2 NCs, which is immobilized onto side-polished AgE with conducting binders for the first time. NCs are prepared extensively using hydrothermal method with reducing agents in alkaline medium, which represents a simple and economical approach. Analytical performances of methanol chemical sensor are investigated by reliable *I–V* method in terms of sensitivity, detection limit in short response time as well as reproducibility. This extensive research is performed in terms of preparation and characterization of doped NCs and applied for the methanol sensor using *I–V* method. Hence, this approach is introduced a new route for efficient chemical sensor development in environmental and healthcare fields.

Acknowledgments

Center of Excellence for Advanced Materials (CEAMR) and Chemistry Department, King Abdulaziz University, Jeddah is highly acknowledged. Authors are thankful to the Deanship of Scientific Research and Centre for Advanced Materials and Nano-Engineering (CAMNE), Najran University, Najran, Saudi Arabia.

References

[1] Y.W. Heo, J. Kelly, D.P. Norton, A.F. Hebard, S.J. Pearton, J.M. Zavada, L.A. Boatner, Electrochem. Solid State Lett. 7 (2004) 309.
[2] E. Comini, G. Faglia, G. Sberveglieri, Z. Pan, Z.L. Wang, Appl. Phys. Lett. 81 (1869) 2002.
[3] M.W.J. Prins, K.O. Grosse-Holz, G. Muller, J.F.M. Cillessen, J.B. Giesbers, R.P. Weening, R.M. Wolf, Appl. Phys. Lett. 68 (1996) 3650.
[4] S.R. Lee, M.M. Rahman, K. Sawada, M. Ishida, Biosens. Bioelectron. 24 (2009) 1877.
[5] A. Umar, M.M. Rahman, S.H. Kim, Y.B. Hahn, Chem. Commun. (2008) 166.
[6] M.M. Rahman, A. Umar, K. Sawada, Sens. Actuators B 137 (2009) 327.
[7] M.M. Rahman, Sens. Transduc. J. 126 (2011) 11.
[8] S.R. Lee, M.M. Rahman, M. Ishida, K. Sawada, Trends Anal. Chem. 28 (2009) 196.
[9] M.M. Rahman, A. Jamal, S.B. Khan, M. Faisal, J. Phys. Chem. C 115 (2011) 9503.
[10] M.M. Rahman, A. Jamal, S.B. Khan, M. Faisal, Biosens. Bioelectron. 28 (2011) 127.
[11] H.L. Hartnagel, A.L. Dawar, A.K. Jain, C. Jagadish, Semiconducting Transparent Thin Films, Institute of Physics, Bristol, UK, 1995.
[12] S.A. Wolf, D.D. Awschalom, R.A. Buhrman, J.M. Daughton, S.V. Molnar, M.L. Roukes, A.Y. Chtchelkanova, D.M. Treger, Science 294 (2001) 1488.
[13] I. Malajovich, J.J. Berry, N. Samarth, Nature 411 (2001) 770.
[14] H. Ohno, Science 281 (1998) 951.
[15] T. Diet, Semicond. Sci. Technol. 17 (2002) 377.
[16] S. Pabchanda, J. Putpan, R. Laopaiboon, UBU J. 12 (1953) 21.
[17] V. Geraldo, J. Europ, Ceram. Soc. 25 (2005) 2825.
[18] M. Batzill, U. Diebold, Prog. Surf. Sci. 79 (2005) 47.
[19] A.B. Bhise, J. Cryst. Growth 307 (2007) 87.
[20] H. Kimura, Appl. Phys. Lett. 80 (2002) 94.
[21] J.M. Coey, M. Venkatesan, C.B. Fitzgerald, Nat. Mater. 4 (2005) 173.
[22] C.X. Xu, Appl. Phys. Lett. 86 (2005) 173110.
[23] J. Sundqvist, J. Lu, M. Ottosson, A. Hårsta, Thin Solid Films 514 (2006) 63.
[24] M.A. Ponce, J. Mater. Sci. Mater. Electron. 18 (2007) 1171.
[25] K. Galatsis, Sens. Actuators B 93 (2003) 562.
[26] M. Seo, Y. Akutsu, H. Kagemoto, Ceram. Int. 33 (2007) 625.
[27] G. Korotcenkov, V. Brinzari, I. Boris, J. Mater. Sci. 43 (2008) 2761.
[28] E. Elangovan, K. Ramamurthi, Thin Solid Films 476 (2005) 231.
[29] X.L. Cheng, H. Zhao, L.H. Huo, S. Gao, J.G. Zhao, Sens. Actuators B 102 (2004) 248.
[30] K. Arshak, I. Gaiden, Mater. Sci. Eng. B 118 (2005) 44.
[31] G. Neri, A. Bonavita, G. Rizzo, S. Galvagno, S. Capone, P. Siciliano, Sens. Actuators B 114 (2005) 687.
[32] N.G. Patel, P.D. Patel, V.S. Vaishnav, Sens. Actuators B 96 (2003) 180.
[33] S. Das, D.Y. Kim, C.M. Choi, Y.B. Hahn, Mater. Res. Bull. 46 (2011) 609.
[34] K.Y. Rajpure, Mater. Chem. Phys. 64 (2000) 184.
[35] M.M. Bagheri-Mohagheghi., Solid State Sci. 11 (2009) 233.
[36] T. Minami, Mater. Res. Soc. Bull. 25 (2000) 38.
[37] A.I. Martinez, D.R. Acosta, Thin Solid Films 483 (2005) 107.
[38] G. Korotcenkov, Process. Appl. Ceram. 3 (2009) 19.
[39] R.W. Joyner, S. Van, Elementary Reaction Steps in Heterogeneous Catalysis, Kluwer Academic Publishers, Netherland, 1993.
[40] J. Mu, B. Chen, Z. Guo, M. Zhang, Z. Zhang, C. Shao, Y. Liu, J. Colloid Interface Sci. 356 (2011) 706.
[41] Y. Liu, F. Yang, X. Yang, Colloid Surf. A: Physicochem. Eng. Aspects 312 (2008) 219.
[42] M.M. Rahman, A. Jamal, S.B. Khan, M. Faisal, ACS Appl. Mater. Interface 3 (2011) 1346.
[43] S.B. Khan, M. Faisal, M.M. Rahman, A. Jamal, Talanta 85 (2011) 943.
[44] M.M. Rahman, A. Jamal, S.B. Khan, M. Faisal, J. Nanopart. Res. 13 (2011) 3789.
[45] D. Lei, M. Zhang, Q. Hao, L. Chen, Q. Li, E. Zhang, T. Wang, Mater. Lett. 65 (2011) 1154.
[46] H.S. Zhuang, H.L. Xia, T. Zhang, D.C. Xiao, Mater. Sci. Polym. 26 (2008) 517.
[47] M. Jayalakshmi, K. Balasubramanian, Int. J. Electrochem. Sci. 4 (2009) 878.
[48] L.M. Fang, J. Alloys Compd. 454 (2008) 261.
[49] T. Krishnakumar, J. Phys. Chem. Solid 70 (2009) 993.
[50] A. Azam, A.S. Ahmed, M.S. Ansari, M. Shafeeq, A.H. Naqvi, J. Alloys Compd. 506 (2010) 237.
[51] A.L. Patterson, Phys. Rev. Online Arch. (Prola) 56 (1939) 978.
[52] J.K. Srivastava, P. Pandey, V.N. Mishra, R. Dwivedi, J. Nat. Gas Chem. 20 (2011) 179.
[53] P.P. Sahay, S. Tewari, S. Jha, M. Shamsuddin, J. Mater. Sci. 40 (2005) 4791.
[54] F. Hellegouarch, F. Arefi-Khonsari, R. Planade, J. Amouroux, Sens. Actuators B 73 (2001) 27.
[55] P.P. Sahay, J. Mater. Sci. 40 (2005) 4383.
[56] A.O. Dikovska, G.B. Atanasova, N.N. Nedyalkov, P.K. Stefanov, P.A. Atanasov, E.I. Karakolev, A.T. Andreev, Sens. Actuators B 146 (2010) 331.
[57] M. Choudhury, S.S. Nath, D. Chakdar, G. Gope, R.K. Nath, Adv. Sci. Lett. 3 (2010) 6.
[58] C.C. Wang, Y.C. Weng, T.C. Chou, Sens. Actuators B 122 (2007) 591.
[59] G. Lia, N.Z. Ma, Y. Wang, Sens. Actuators B 109 (2005) 285.